Supplementary Information

Supplementary Results 1. Optical power and efficiency distributions of μLEDs fabricated on wafers with Si substrates with different doping densities

Electrical and optical characteristics of μLEDs fabricated on GaN-on-Si GaN/InGaN MQW LED wafers with different doping densities were measured and compared. After the current and optical flux values were measured at varying LED bias voltages from 0 V to 4 V, current at forward bias voltage of 4 V (I(V = 4 V)), optical flux generated from forward bias of 4 V (E_e(V = 4 V)), and the peak plug efficiency (max(η_{plug})) of each LED were calculated and compared.

Contrary to our initial conjecture that the efficiency and therefore the maximum output optical flux of LEDs on heavily boron doped silicon substrate will be lower than those of the LEDs on intrinsic silicon substrate due to increased defect density inside the silicon substrate, the efficiency of the LEDs on the intrinsic silicon substrate were the lowest (Supplementary Figure 4a-c). However, considering large variation of LED characteristics even within the same substrate (Supplementary Figure 4d-f), it is difficult to conclude that the doping density of the silicon substrate has significant effect on the electrical and the optical characteristics of the LEDs and therefore the efficiency.

Supplementary Methods

Supplementary Methods 1. Characterization of optical power and efficiency distributions of μLEDs fabricated on wafers with Si substrates with different doping densities

Simple μLED test structures were built using the process similar to fabrication process for μLED optoelectrodes. After formation of μLED structures, whose LED mesa dimensions are identical to those on the μLED optoelectrodes, the 4" GaN-on-Si GaN/InGaN MQW LED wafers with the μLED test structures were diced into small (4 × 10 mm) pieces each of which contains nine μLEDs. The pieces were then mounted on the PCBs and connected in the same way as the actual μLED optoelectrodes are connected to the PCBs.

The electrical and optical characteristics of each μLED on the μLED test structures were characterized using the setup and the procedure identical to those for characterization of the actual μLED optoelectrodes, outlined in Methods.

Supplementary Methods 2. *In vitro* characterization of photovoltaic-effect-induced artifact on μLED optoelectrodes and electrode arrays on non-Si substrates

Identical to characterization of LED-driving induced stimulation artifact, characterization of photovoltaic-effect-induced artifact was conducted in 1 × PBS solution (prepared using 10 × PSB purchased from MP Biomedicals, Solon, OH). A fiber optic cannula (CFMXD10, Thorlabs, Newton, NJ) was attached to a clear plastic container (Container Store, Coppel, TX) through a hole drilled on a side of the container using a 3D printed frame and glue. PBS was poured so that the exposed optical fiber tip of the cannula is submerged approximately 2.5 mm under the surface of the PBS. The optoelectrode, attached to a 3-axis micromanipulator on a stereotaxic frame (Model 962, David Kopf Instruments, Tujunga, CA), was lowered into the container until the shanks were sufficiently submerged into the PBS. The position of the optoelectrode was precisely adjusted using the micromanipulator so that the tips of

the optoelectrode are exactly 1.5 mm away from the tip of the optical fiber, while the top side of the optoelectrode which has the electrodes and the μLED are facing the optical fiber.

Optical stimulation was provided using a fiber-coupled LED light source (M470F3, Thorlabs), whose spectrum is similar to those of the μLEDs (λ_{peak} = 470 nm). Optical power at the end of the fiber optic cannula was pre-measured using the combination of the integrating sphere and the spectrometer. 5-Hz, 50-ms long (25 % duty ratio) rectangular voltage pulses with varying on-voltage levels were used as the LED driving signal. Pulses with 0 V low-level (off-time) voltage and high-level (on-time) voltage that would generate the irradiance same as the pre-characterized irradiance was used.

Intan RHD2132 neural signal amplifier headstage PCB (RHD2132, Intan Technologies, Los Angeles, CA) recorded the stimulation artifact signal. Data collection and processing followed the procedure identical to that has been previously outlined in the Methods for LED-driving-induced stimulation artifact characterization.

Supplementary Methods 3. Electrostatics simulation for calculation of mutual capacitances between interconnects

COMSOL Multiphysics (COMSOL Inc., Burlington, MA) was used for finite element analysis of mutual capacitance distribution among the metal traces (interconnects) on the shanks of the μLED optoelectrode. A 2D model of the shank was built by drawing the cross-section of the optoelectronic shank, and electrostatics physics interface was imported to calculate the mutual capacitance values of 100-μm long segments of the of the shanks of μLED optoelectrodes with and without shielding layers. Built-in material properties (dielectric constants) of air and silicon dioxide were used. Each interconnect plus the n-GaN layer was assigned either terminal (V = 0) or floating potential (Q = 0) boundary conditions. For the mutual capacitance values, the Maxwell capacitance matrix was calculated using automatic terminal weep and the mutual capacitance values were extracted and reported. For

capacitive coupling magnitude, all the boundaries that correspond to the recording electrode interconnects were defined as terminals with floating potential, all the boundaries that correspond to the LED ground (cathode) interconnects and the shielding layers were defined as grounds (V = 0) and, assuming the LED and n-GaN voltages of 1 V, the voltage values (in dB) were reported.

Supplementary Methods 4. Device physics simulation for calculation of photovoltacially induced electrostatic potential buildup inside silicon substrate

Sentaurus TCAD suite (Synopsis, Mountain View, CA) was used for finite element analysis of carrier generation and electrostatic potential buildup inside the silicon substrate of the μLED optoelectrode during illumination. A 3D model of the silicon shank was built using Sentaurus Device Editor and was given different boron doping densities. Two contacts, each of which indicate GaN-AlN interface and the silicon-PBS interface, were created and appropriately assigned. Using Sentaurus Device, carrier distribution and electrostatic potential buildup during irradiation of specified intensity were calculated. Coupled Poisson equations for electrons and holes were solved in the time domain with assumption of density-dependent Shockley-Read-Hall recombination. Voltage of the contact for silicon-PBS interface before, during, and after the specified irradiation and optical generation of electrons and holes were recorded and reported.

Supplementary Table 1: Summary of the experimental conditions used for each type of experiment for characterization of stimulation artifact.

Type of experiment		Effect of shielding layer	Effect of substrate doping	Effect of slew rate
Devices used		2 × non-shielded, p^--Si substrate; 2 × shielded, p^--Si substrate	2 × shielded, FZ-Si substrate; 2 × shielded, p^--Si substrate; 2 × shielded, p^+-Si substrate	2 × shielded, p^+-Si substrate
LED signal	**Low-level voltage (V)**	0	0	0, 2.8
	High-level voltage (V)	[2.71 ± 0.02, 3.36 ± 0.09] (mean ± SD)	[2.76 ± 0.11, 3.57 ± 0.15] (mean ± SD)	3.5
	Equivalent on-time irradiance (mW mm^{-2})	1, 2, 5, 10, 20, 30, 40, 50	1, 2, 5, 10, 20, 30, 40, 50	40.39 ± 10.73 (mean ± SD)
	Pulse rise time (10 - 90 %)	5 ns	5 ns	5 ns, 10 ns, 50 ns, 100 ns, 500 ns, 1 μs, 5 μs, 10 μs, 50 μs, 100 μs, 500 μs, 1 ms

Supplementary Table 2: List of the statistical tests of significance used in the study.

Figure (panel)	**Fig. 3b**
Test used	Mann-Whitney U test with Bonferroni correction
Samples and categories	Peak-to-peak magnitudes of stimulation artifact, recorded from all sites on the 1st-generation (i.e. non-shielded with moderate boron doping of the silicon substrate) μLED optoelectrodes, measured during optical stimulation using the μLEDs resulting in output irradiance of 1, 2, 5, 10, 20, 30, 40 and 50 mW mm^{-2}
Statistics provided in figure	Box plots with whiskers and outliers (denoting median, IQR, EVs and outliers)
n	75 (for all categories)
p-values	2.84×10^{-1} (1 vs. 2 mW mm^{-2}), 3.25×10^{-2} (2 vs. 5 mW mm^{-2}), 3.89×10^{-3} (5 vs. 10 mW mm^{-2}), 7.87×10^{-3} (10 vs. 20 mW mm^{-2}), 1.63×10^{-2} (20 vs. 30 mW mm^{-2}), 3.61×10^{-1} (30 vs. 40 mW mm^{-2}), & 2.48×10^{-3} (40 vs. 50 mW mm^{-2})
Other values	z = -1.07 (1 vs. 2 mW mm^{-2}), 2.14 (2 vs. 5 mW mm^{-2}), -2.89 (5 vs. 10 mW mm^{-2}), 2.66 (10 vs. 20 mW mm^{-2}), -2.40 (20 vs. 30 mW mm^{-2}), 9.13×10^{-1} (30 vs. 40 mW mm^{-2}), & -3.03 (40 vs. 50 mW mm^{-2})

Figure (panel)	**Fig. 3e**
Test used	Mann-Whitney U test with Bonferroni correction
Samples and categories	Peak-to-peak magnitudes of stimulation artifact, recorded from all sites on shielded μLED optoelectrodes fabricated using LED wafer with moderately boron-doped silicon substrate, measured during optical stimulation using the μLEDs resulting in output irradiance of 1, 2, 5, 10, 20, 30, 40 and 50 mW mm^{-2}
Statistics provided in figure	Box plots with whiskers and outliers (denoting median, IQR, EVs and outliers)
n	67 (for all categories)
p-values	1.76×10^{-1} (1 vs. 2 mW mm^{-2}), 9.70×10^{-2} (2 vs. 5 mW mm^{-2}), 4.03×10^{-6} (5 vs. 10 mW mm^{-2}), 3.51×10^{-10} (10 vs. 20 mW mm^{-2}), 1.88×10^{-7} (20 vs. 30 mW mm^{-2}), 2.23×10^{-5} (30 vs. 40 mW mm^{-2}), & 2.48×10^{-3} (40 vs. 50 mW mm^{-2})
Other values	z = 1.35 (1 vs. 2 mW mm^{-2}), -1.66 (2 vs. 5 mW mm^{-2}), -4.61 (5 vs. 10 mW mm^{-2}), -6.27 (10 vs. 20 mW mm^{-2}), -5.21 (20 vs. 30 mW mm^{-2}), -4.24 (30 vs. 40 mW mm^{-2}), & -3.03 (40 vs. 50 mW mm^{-2})

Figure (panel)	**Fig. 3g**
Test used	Mann-Whitney U test
Samples and categories	Peak-to-peak magnitudes of stimulation artifact, recorded from all sites on the 1st-generation (i.e. non-shielded with moderate boron doping of the silicon substrate) μLED optoelectrodes and shielded μLED optoelectrodes fabricated using LED wafer with moderately boron-doped silicon substrate, measured during optical stimulation using the μLEDs resulting in output irradiance of 1, 2, 5, 10, 20, 30, 40 and 50 mW mm^{-2}

Statistics provided in figure	Scatter plots with error bars (denoting mean and SD)
n	75 and 67 (for all categories)
p-values	4.09×10^{-23} (@ 1 mW mm^{-2}), 3.07×10^{-23} (@ 2 mW mm^{-2}), 9.70×10^{-24} (@ 5 mW mm^{-2}), 5.20×10^{-24} (@ 10 mW mm^{-2}), 2.18×10^{-17} (@ 20 mW mm^{-2}), 8.72×10^{-22} (@ 30 mW mm^{-2}), 2.81×10^{-15} (@ 40 mW mm^{-2}), & 2.72×10^{-23} (@ 50 mW mm^{-2})
Other values	z = 9.90 (@ 1 mW mm^{-2}), 9.93 (@ 2 mW mm^{-2}), 1.00×10^{1} (@ 5 mW mm^{-2}), 8.48 (@ 10 mW mm^{-2}), 9.59 (@ 20 mW mm^{-2}), 7.90 (@ 30 mW mm^{-2}), 7.90 (@ 40 mW mm^{-2}), & 9.94 (@ 50 mW mm^{-2})

Figure (panel)	**Fig. 4a, left**
Test used	Mann-Whitney U test with Bonferroni correction
Samples and categories	Peak-to-peak magnitudes of stimulation artifact, recorded from all sites on shielded μLED optoelectrodes fabricated using LED wafer with FZ-silicon substrate, measured during optical stimulation using the μLEDs resulting in output irradiance of 1, 2, 5, 10, 20, 30, 40 and 50 mW mm^{-2}
Statistics provided in figure	Box plots with whiskers and outliers (denoting median, IQR, EVs and outliers)
n	124 (for all categories)
p-values	1.98×10^{-15} (1 vs. 2 mW mm^{-2}), 4.91×10^{-28} (2 vs. 5 mW mm^{-2}), 5.67×10^{-13} (5 vs. 10 mW mm^{-2}), 2.81×10^{-8} (10 vs. 20 mW mm^{-2}), 8.95×10^{-3} (20 vs. 30 mW mm^{-2}), 5.29×10^{-2} (30 vs. 40 mW mm^{-2}), & 9.61×10^{-1} (40 vs. 50 mW mm^{-2})
Other values	z = -7.94 (1 vs. 2 mW mm^{-2}), -1.10×10^{1} (2 vs. 5 mW mm^{-2}), -7.21 (5 vs. 10 mW mm^{-2}), -5.55 (10 vs. 20 mW mm^{-2}), -2.61 (20 vs. 30 mW mm^{-2}), -1.94 (30 vs. 40 mW mm^{-2}), & -4.87×10^{-2} (40 vs. 50 mW mm^{-2})

Figure (panel)	**Fig. 4a, center**
Test used	Mann-Whitney U test with Bonferroni correction
Samples and categories	Peak-to-peak magnitudes of stimulation artifact, recorded from all sites on shielded μLED optoelectrodes fabricated using LED wafer with moderately boron-doped silicon substrate, measured during optical stimulation using the μLEDs resulting in output irradiance of 1, 2, 5, 10, 20, 30, 40 and 50 mW mm^{-2}
Statistics provided in figure	Box plots with whiskers and outliers (denoting median, IQR, EVs and outliers)
n	67 (for all categories)
p-values	1.76×10^{-1} (1 vs. 2 mW mm^{-2}), 9.70×10^{-2} (2 vs. 5 mW mm^{-2}), 4.03×10^{-6} (5 vs. 10 mW mm^{-2}), 3.51×10^{-10} (10 vs. 20 mW mm^{-2}), 1.88×10^{-7} (20 vs. 30 mW mm^{-2}), 2.23×10^{-5} (30 vs. 40 mW mm^{-2}), & 2.48×10^{-3} (40 vs. 50 mW mm^{-2})
Other values	z = 1.35 (1 vs. 2 mW mm^{-2}), -1.66 (2 vs. 5 mW mm^{-2}), -4.61 (5 vs. 10 mW mm^{-2}), -6.27 (10 vs. 20 mW mm^{-2}), -5.21 (20 vs. 30 mW mm^{-2}), -4.24 (30 vs. 40 mW mm^{-2}), & -3.03 (40 vs. 50 mW mm^{-2})

Figure (panel)	**Fig. 4a, right**
Test used	Mann-Whitney U test with Bonferroni correction
Samples and categories	Peak-to-peak magnitudes of stimulation artifact, recorded from all sites on shielded μLED optoelectrodes fabricated using LED wafer with heavily boron-doped silicon substrate, measured during optical stimulation using the μLEDs resulting in output irradiance of 1, 2, 5, 10, 20, 30, 40 and 50 mW mm^{-2}
Statistics provided in figure	Box plots with whiskers and outliers (denoting median, IQR, EVs and outliers)
n	151 (for all categories)
p-values	9.61×10^{-1} (1 vs. 2 mW mm^{-2}), 5.22×10^{-1} (2 vs. 5 mW mm^{-2}), 6.05×10^{-1} (5 vs. 10 mW mm^{-2}), 8.68×10^{-1} (10 vs. 20 mW mm^{-2}), 6.46×10^{-1} (20 vs. 30 mW mm^{-2}), 4.78×10^{-1} (30 vs. 40 mW mm^{-2}), & 5.54×10^{-1} (40 vs. 50 mW mm^{-2})
Other values	$z = 4.88 \times 10^{-2}$ (1 vs. 2 mW mm^{-2}), 6.41×10^{-1} (2 vs. 5 mW mm^{-2}), 5.17×10^{-1} (5 vs. 10 mW mm^{-2}), -1.66×10^{-1} (10 vs. 20 mW mm^{-2}), -4.60×10^{-1} (20 vs. 30 mW mm^{-2}), -7.09×10^{-1} (30 vs. 40 mW mm^{-2}), & -5.92×10^{-1} (40 vs. 50 mW mm^{-2})

Figure (panel)	**Fig. 6b**
Test used	Mann-Whitney U test with Bonferroni correction
Samples and categories	Peak-to-peak magnitudes of stimulation artifact, recorded from all sites on control μLED optoelectrodes (i.e. non-shielded optoelectrodes with moderate boron doping of the silicon substrate, C), optoelectrodes with shielding layer and moderately boron-doped the silicon substrate (S-p^-), and the optoelectrodes with shielding layer and heavily boron-doped silicon substrate (S-p^+)
Statistics provided in figure	Box plots with whiskers and outliers (denoting median, IQR, EVs and outliers)
n	75 (C), 67 (S-p^-), & 151 (S-p^+)
p-values	2.71×10^{-23} (C vs. S-p^-), 2.93×10^{-34} (C vs. S-p^+), & 5.64×10^{-24} (S-p^- vs. S-p^+)
Other values	$z = 9.94$ (C vs. S-p^-), 122.05 (C vs. S-p^+), & 100.98 (S-p^- vs. S-p^+)

Figure (panel)	**Fig. 7b, left**
Test used	Mann-Whitney U test with Bonferroni correction
Samples and categories	Peak-to-peak magnitudes of stimulation artifact, recorded from all sites on shielded μLED optoelectrodes fabricated using LED wafer with FZ-silicon substrate (FZ-Si), shielded μLED optoelectrodes fabricated using LED wafer with moderately boron-doped silicon substrate (p^--Si), and shielded μLED optoelectrodes fabricated using LED wafer with heavily boron-doped silicon substrate (p^+-Si)
Statistics provided in figure	Box plots with whiskers and outliers (denoting median, IQR, EVs and outliers)
n	124 (FZ-Si), 67 (p^--Si), & 151 (p^+-Si)
p-values	1.30×10^{-5} (p^--Si vs. FZ-Si) & 5.64×10^{-24} (p^--Si vs. p^+-Si)
Other values	$z = -4.36$ (p^--Si vs. FZ-Si) & 100.98 (p^--Si vs. p^+-Si)

Figure (panel)	**Fig. 7b, center**
Test used	Mann-Whitney U test with Bonferroni correction
Samples and categories	Peak-to-peak magnitudes of stimulation artifact, recorded from two sites at the bottom of each shank (sites 1 & 2) on shielded μLED optoelectrodes fabricated using LED wafer with FZ-silicon substrate (FZ-Si), shielded μLED optoelectrodes fabricated using LED wafer with moderately boron-doped silicon substrate (p^--Si), and shielded μLED optoelectrodes fabricated using LED wafer with heavily boron-doped silicon substrate (p^+-Si)
Statistics provided in figure	Box plots with whiskers and outliers (denoting median, IQR, EVs and outliers)
n	34 (FZ-Si), 19 (p^--Si), & 38 (p^+-Si)
p-values	1.19×10^{-2} (p^--Si vs. FZ-Si) & 9.53×10^{-1} (p^--Si vs. p^+-Si)
Other values	z = -2.51 (p^--Si vs. FZ-Si) & 4.92×10^{-2} (p^--Si vs. p^+-Si)

Figure (panel)	**Fig. 7b, right**
Test used	Mann-Whitney U test with Bonferroni correction
Samples and categories	Peak-to-peak magnitudes of stimulation artifact, recorded from two sites at the top of each shank (sites 7 & 8) on shielded μLED optoelectrodes fabricated using LED wafer with FZ-silicon substrate (FZ-Si), shielded μLED optoelectrodes fabricated using LED wafer with moderately boron-doped silicon substrate (p^--Si), and shielded μLED optoelectrodes fabricated using LED wafer with heavily boron-doped silicon substrate (p^+-Si)
Statistics provided in figure	Box plots with whiskers and outliers (denoting median, IQR, EVs and outliers)
n	32 (FZ-Si), 22 (p^--Si), & 41 (p^+-Si)
p-values	1.32×10^{-5} (p^--Si vs. FZ-Si) & 8.29×10^{-11} (p^--Si vs. p^+-Si)
Other values	z = -4.36 (p^--Si vs. FZ-Si) & 6.50 (p^--Si vs. p^+-Si)

Figure (panel)	**Fig. 7e, bottom**
Test used	Mann-Whitney U test
Samples and categories	Peak-to-peak magnitudes of stimulation artifact, recorded different sites on each shank (sites 1 - 8) on shielded μLED optoelectrodes fabricated using LED wafer with heavily boron-doped silicon substrate
Statistics provided in figure	Box plots with whiskers and outliers (denoting median, IQR, EVs and outliers)
n	22 (site 1), 16 (site 2), 12 (site 3), 22 (site 4), 20 (site 5), 18 (site 6), 22 (site 7), & 19 (site 8)
p-values	7.79×10^{-1} (site 1 vs. 2), 3.97×10^{-1} (site 3 vs. 4), 5.93×10^{-2} (site 5 vs. 6), & 5.05×10^{-1} (site 7 vs. 8)
Other values	z = 2.81×10^{-1} (site 1 vs. 2), 8.47×10^{-1} (site 3 vs. 4), 1.89 (site 5 vs. 6), & -6.67×10^{-1} (site 7 vs. 8)

Figure (panel)	**Fig. 7e, top**
Test used	Mann-Whitney U test with Bonferroni correction
Samples and categories	Peak-to-peak magnitudes of stimulation artifact, recorded different sites on each shank (sites 1 - 8) on shielded μLED optoelectrodes fabricated using LED wafer with heavily boron-doped silicon substrate
Statistics provided in figure	Box plots with whiskers and outliers (denoting median, IQR, EVs and outliers)
n	38 (site 1 & 2), 44 (site 3 & 4), 38 (site 5 & 6), & 41 (site 7 & 8)
p-values	4.65×10^{-11} (site 1 & 2 vs. sites 3 & 4), 1.41×10^{-4} (site 3 & 4 vs. sites 5 & 6), & 6.99×10^{-4} (site 5 & 6 vs. sites 7 & 8)
Other values	z = 6.58 (site 1 & 2 vs. sites 3 & 4), 3.81 (site 3 & 4 vs. sites 5 & 6), & 3.39 (site 5 & 6 vs. sites 7 & 8)

Figure (panel)	**Fig. 8d**
Test used	Mann-Whitney U test with Bonferroni correction
Samples and categories	Peak-to-peak magnitudes of stimulation artifact, recorded from two sites at the bottom of each shank (sites 1 & 2) on shielded μLED optoelectrodes fabricated using LED wafer with heavily boron-doped silicon substrate during LED driving with voltage pulses with 0 V low-level voltage and 5 ns rise time (0V-5ns), with pulses with 0 V low-level voltage and 1 ms rise time (0V-1ms), with pulses with 2.8 V low-level voltage and 5 ns rise time (2P8V-4ns), and with pulses with 2.8V low-level voltage and 1 ms rise time (2P8V-1ms)
Statistics provided in figure	Box plots with whiskers (denoting median, IQR, and EVs)
n	35 (for all categories)
p-values	1.98×10^{-12} (0V-5ns vs. 0V-1ms), 6.55×10^{-13} (0V-5ns vs. 2P8V-5ns), & 6.55×10^{-13} (0V-5ns vs. 2P8V-1ms)
Other values	z = 7.04 (0V-5ns vs. 0V-1ms), 7.19 (0V-5ns vs. 2P8V-5ns), & 7.19 (0V-5ns vs. 2P8V-1ms)

Figure (panel)	**Supplementary Fig. 2c**
Test used	Mann-Whitney U test with Bonferroni correction
Samples and categories	Peak-to-peak magnitudes of PV-induced voltage signal, recorded from all sites on shielded μLED optoelectrodes fabricated using LED wafer with FZ-silicon substrate (FZ-Si), shielded μLED optoelectrodes fabricated using LED wafer with moderately boron-doped silicon substrate (p^--Si), and shielded μLED optoelectrodes fabricated using LED wafer with heavily boron-doped silicon substrate (p^+-Si)
Statistics provided in figure	Box plots with whiskers (denoting median, IQR, and EVs)
n	55 (FZ-Si), 49 (p^--Si), & 56 (p^+-Si)
p-values	1.76×10^{-18} (FZ-Si vs. p^--Si), 1.86×10^{-18} (FZ-Si vs. p^+-Si), & 1.26×10^{-18} (p^--Si vs. p^+-Si)
Other values	z = -8.77 (FZ-Si vs. p^--Si), 9.02 (FZ-Si vs. p^+-Si), & 8.81 (p^--Si vs. p^+-Si)

Figure (panel)	**Supplementary Fig. 3c**
Test used	Mann-Whitney U test with Bonferroni correction
Samples and categories	Peak-to-peak magnitudes of PV-induced voltage signal, recorded from all sites on shielded μLED optoelectrodes fabricated using LED wafer with heavily boron-doped silicon substrate (p^+-Si), electrode arrays fabricated using soda-lime glass substrate (G), and electrode arrays fabricated using LED-on-sapphire substrate (S)
Statistics provided in figure	Box plots with whiskers (denoting median, IQR, and EVs)
n	56 (p^+-Si), 20 (G), & 26 (S)
p-values	4.11×10^{-11} (p^+-Si vs. G), 4.19×10^{-13} (p^+-Si vs. S), & 2.60×10^{-2} (G vs. S)
Other values	z = 6.60 (p^+-Si vs. G), 7.25 (p^+-Si vs. S), & -2.23 (G vs. S)

Figure (panel)	**Supplementary Fig. 4a**
Test used	Mann-Whitney U test with Bonferroni correction
Samples and categories	Current through μLEDs fabricated on LED wafer with FZ-silicon substrate (FZ-Si), μLEDs fabricated on LED wafer with moderately boron-doped silicon substrate (p^--Si), and μLEDs fabricated on LED wafer with heavily boron-doped silicon substrate (p^+-Si), at 4 V of forward bias voltage
Statistics provided in figure	Box plots with whiskers and outliers (denoting median, IQR, EVs and outliers)
n	43 (FZ-Si), 44 (p^--Si), & 43 (p^+-Si)
p-values	3.01×10^{-5} (FZ-Si vs. p^--Si), 1.34×10^{-5} (FZ-Si vs. p^+-Si), & 2.68×10^{-1} (p^--Si vs. p^+-Si)
Other values	z = -4.17 (FZ-Si vs. p^--Si), -4.35 (FZ-Si vs. p^+-Si), & -1.11 (p^--Si vs. p^+-Si)

Figure (panel)	**Supplementary Fig. 4b**
Test used	Mann-Whitney U test with Bonferroni correction
Samples and categories	Optical flux generated from μLEDs fabricated on LED wafer with FZ-silicon substrate (FZ-Si), μLEDs fabricated on LED wafer with moderately boron-doped silicon substrate (p^--Si), and μLEDs fabricated on LED wafer with heavily boron-doped silicon substrate (p^+-Si), at 4 V of forward bias voltage
Statistics provided in figure	Box plots with whiskers and outliers (denoting median, IQR, EVs and outliers)
n	43 (FZ-Si), 44 (p^--Si), & 43 (p^+-Si)
p-values	7.52×10^{-6} (FZ-Si vs. p^--Si), 2.62×10^{-6} (FZ-Si vs. p^+-Si), & 3.35×10^{-1} (p^--Si vs. p^+-Si)
Other values	z = -4.48 (FZ-Si vs. p^--Si), -4.70 (FZ-Si vs. p^+-Si), & -9.64×10^{-1} (p^--Si vs. p^+-Si)

Figure (panel)	**Supplementary Fig. 4c**
Test used	Mann-Whitney U test with Bonferroni correction

Samples and categories	Maximum plug efficiency of μLEDs fabricated on LED wafer with FZ-silicon substrate (FZ-Si), μLEDs fabricated on LED wafer with moderately boron-doped silicon substrate (p^--Si), and μLEDs fabricated on LED wafer with heavily boron-doped silicon substrate (p^+-Si)
Statistics provided in figure	Box plots with whiskers and outliers (denoting median, IQR, EVs and outliers)
n	43 (FZ-Si), 44 (p^--Si), & 43 (p^+-Si)
p-values	1.10×10^{-2} (FZ-Si vs. p^--Si), 8.57×10^{-2} (FZ-Si vs. p^+-Si), & 4.52×10^{-1} (p^--Si vs. p^+-Si)
Other values	z = -2.54 (FZ-Si vs. p^--Si), -1.72 (FZ-Si vs. p^+-Si), & -7.51×10^{-1} (p^--Si vs. p^+-Si)

Figure (panel)	**Supplementary Fig. 4d**
Test used	Kruskal-Wallis test
Samples and categories	Current through μLEDs fabricated on LED wafer with FZ-silicon substrate (FZ-Si), μLEDs fabricated on LED wafer with moderately boron-doped silicon substrate (p^--Si), and μLEDs fabricated on LED wafer with heavily boron-doped silicon substrate (p^+-Si), at 4 V of forward bias voltage, measured from five different locations on each wafer (B, C, T, L, and R).
Statistics provided in figure	Box plots with whiskers and outliers (denoting median, IQR, EVs and outliers)
n	8, 9, 9, 9, & 8 (FZ-Si; B, C, T, L, & R); 9, 9, 9, 8, & 9 (p^--Si; B, C, T, L, & R); & 7, 9, 9, 9, & 9 (p^+-Si; B, C, T, L, & R)
p-values	2.67×10^{-2} (FZ-Si), 5.51×10^{-2} (p^--Si), & 7.90×10^{-1} (p^+-Si)
Other value	$\chi^2 = 1.63 \times 10^1$ (FZ-Si), 9.25 (p^--Si), & 1.70 (p^+-Si)

Figure (panel)	**Supplementary Fig. 4e**
Test used	Mann-Whitney U test with Bonferroni correction
Samples and categories	Optical flux generated from μLEDs fabricated on LED wafer with FZ-silicon substrate (FZ-Si), LED wafer with moderately boron-doped silicon substrate (p^--Si), and LED wafer with heavily boron-doped silicon substrate (p^+-Si), at 4 V of forward bias voltage, measured from five different locations on each wafer (B, C, T, L, and R).
Statistics provided in figure	Box plots with whiskers and outliers (denoting median, IQR, EVs and outliers)
n	8, 9, 9, 9, & 8 (FZ-Si; B, C, T, L, & R); 9, 9, 9, 8, & 9 (p^--Si; B, C, T, L, & R); & 7, 9, 9, 9, & 9 (p^+-Si; B, C, T, L, & R)
p-values	6.44×10^{-4} (FZ-Si), 1.52×10^{-3} (p^--Si), & 3.11×10^{-1} (p^+-Si)
Other values	$\chi^2 = 1.94 \times 10^1$ (FZ-Si), 1.75×10^1 (p^--Si), & 4.78 (p^+-Si)

Figure (panel)	**Supplementary Fig. 4f**
Test used	Mann-Whitney U test with Bonferroni correction
Samples and categories	Maximum plug efficiency of μLEDs fabricated on LED wafer with FZ-silicon substrate (FZ-Si), μLEDs fabricated on LED wafer with moderately boron-doped silicon

	substrate (p^--Si), and μLEDs fabricated on LED wafer with heavily boron-doped silicon substrate (p^+-Si), measured from five different locations on each wafer (B, C, T, L, and R).
Statistics provided in figure	Box plots with whiskers and outliers (denoting median, IQR, EVs and outliers)
n	8, 9, 9, 9, & 8 (FZ-Si; B, C, T, L, & R); 9, 9, 9, 8, & 9 (p^--Si; B, C, T, L, & R); & 7, 9, 9, 9, & 9 (p^+-Si; B, C, T, L, & R)
p-values	7.84×10^{-4} (FZ-Si), 3.16×10^{-4} (p^--Si), & 1.47×10^{-5} (p^+-Si)
Other values	$\chi^2 = 1.90 \times 10^1$ (FZ-Si), 2.10×10^1 (p^--Si), & 2.76×10^1 (p^+-Si)

Figure (panel)	**Supplementary Fig. 7c**
Test used	Mann-Whitney U test with Bonferroni correction
Samples and categories	Peak-to-peak magnitudes of stimulation artifact, recorded from two sites at the bottom of each shank (sites 1 & 2) on shielded μLED optoelectrodes fabricated using LED wafer with heavily boron-doped silicon substrate during LED driving with current pulses different shapes – trapezoidal, sinusoidal, and sigmoidal – with 10 - 90 % rise times of approximately 1 ms.
Statistics provided in figure	Box plots with whiskers (denoting median, IQR, and EVs)
n	18 (for all categories)
p-value	9.33×10^{-2}
Other values	$\chi^2 = 4.74$

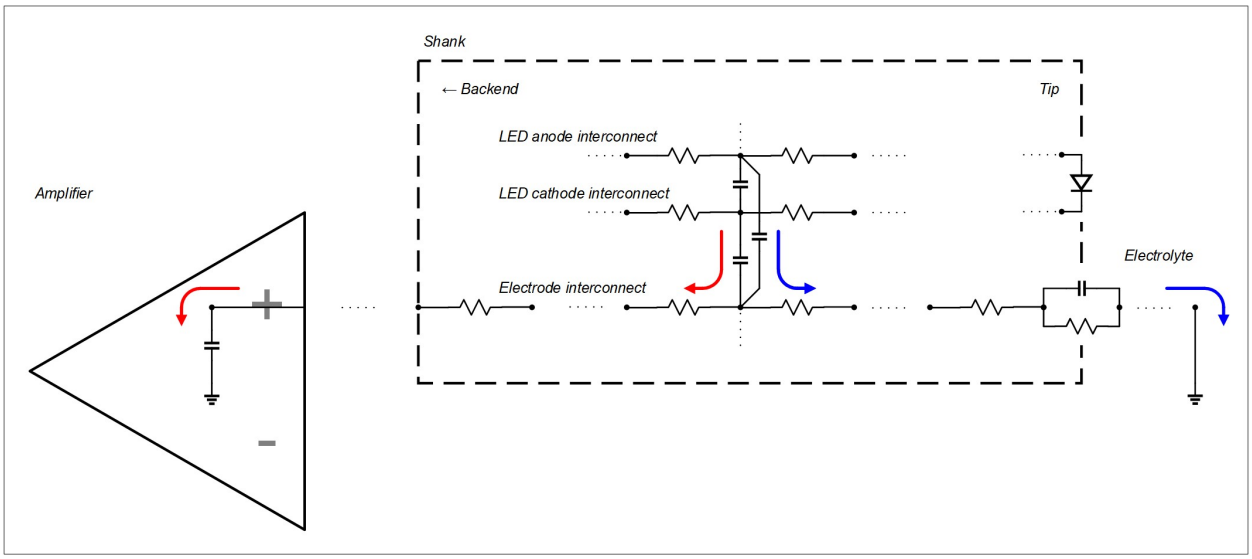

Supplementary Figure 1: Detailed circuit diagram of the neural signal recording circuitry. Detailed equivalent circuit diagram of the neural signal recording circuitry, whose simplified version is presented in Fig. 2b, is shown. A parallel RC component, representing the electrical double layer at the electrode / electrolyte interface, and a capacitor, representing the signal amplifier's input impedance, are shown at the ends of the series resistor components representing the recording electrode interconnect. The current induced due to capacitive voltage coupling, which originates from the LED driving circuitry, is divided into two branches, each of which is highlighted in an arrow of a color. Reduction of the electrode impedance would result in larger current flowing through the branch identified with the blue arrow and, in turn, smaller current flowing through the branch identified with the red arrow. Therefore, with reduced electrode impedance, reduction of the magnitude of the stimulation artifact measured at the amplifier input is expected.

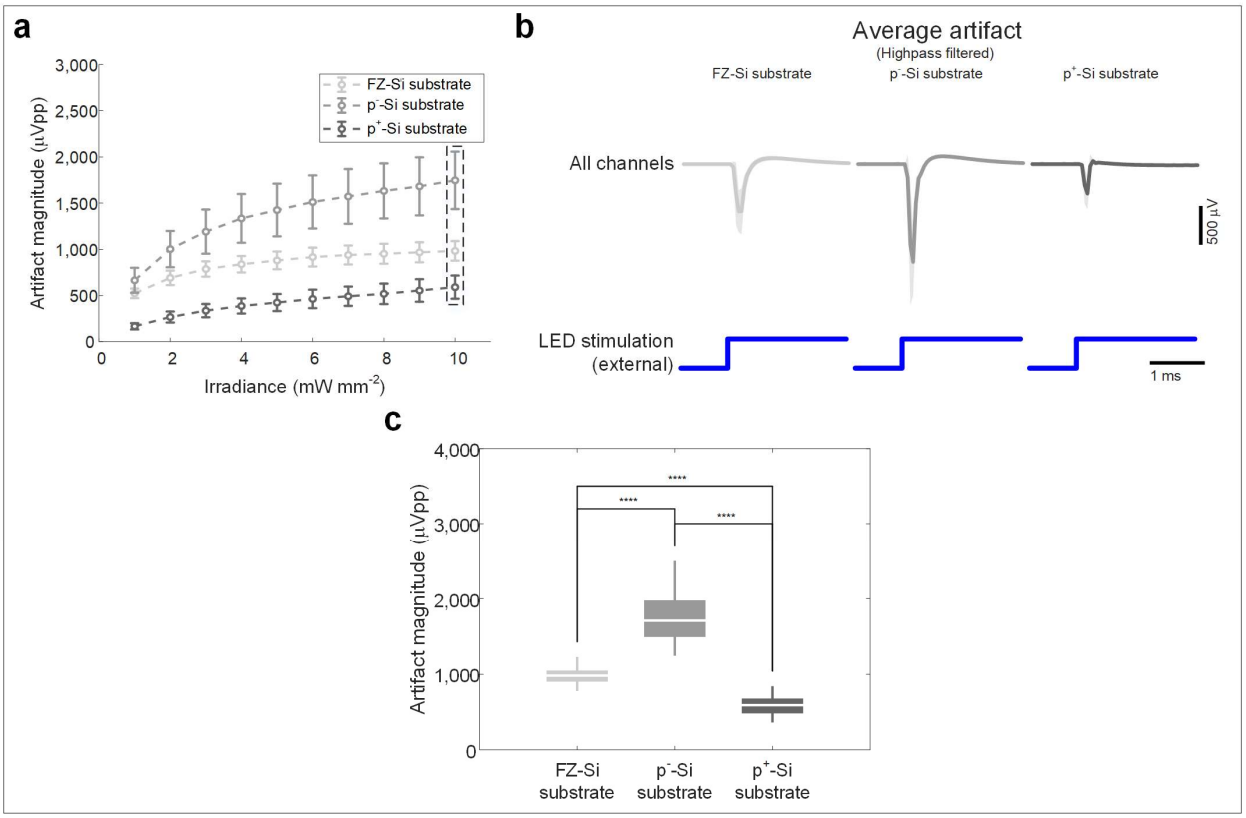

Supplementary Figure 2: PV-induced voltage signals measured from recording electrodes on shielded μLED optoelectrodes fabricated using GaN-on-Si LED wafers with silicon substrates with different boron doping densities. (a) Mean peak-to-peak magnitude of the high-pass filtered PV-induced voltage signal recorded from all the recording channels on shielded μLED optoelectrodes. X coordinates indicate the irradiance of at the surface of the optoelectrode, and the error bars indicate one standard deviation. n = 55, 49, and 56 for devices with FZ-Si substrate, p^--Si substrate, and p^+-Si substrate, respectively. (b) Average high-pass filtered waveforms of PV-induced voltage signal recorded from all the recording channels on the optoelectrode. The irradiance of the LED illumination on the optoelectrode surface was 10 mW mm^{-2}. The shaded regions show one standard deviation away from the mean and the blue traces at the bottom indicate the signal provided to the fiber-coupled LED. The sharp transient component with negative polarity is greatly reduced on the shielded μLED optoelectrodes fabricated using the wafer with heavily-doped silicon substrate. (c) Peak-to-peak magnitudes of the signals whose averages are

plotted in part b. Boxes indicate interquartile ranges, white lines medians, and whiskers extreme values. Mann-Whitney U test was used, and **** indicates $p < 3.33 \times 10^{-5}$. The mean (± SD) peak-to-peak magnitudes are 982.43 (± 105.76), 1746.80 (± 310.89), and 589.72 (± 125.64) μVpp for devices with FZ-Si substrate (n = 55), p^--Si substrate (n = 49), and p^+-Si substrate (n = 56), respectively. Significant reduction of the magnitude of the PV-induced voltage signal with heavy boron doping of the silicon substrate is notable.

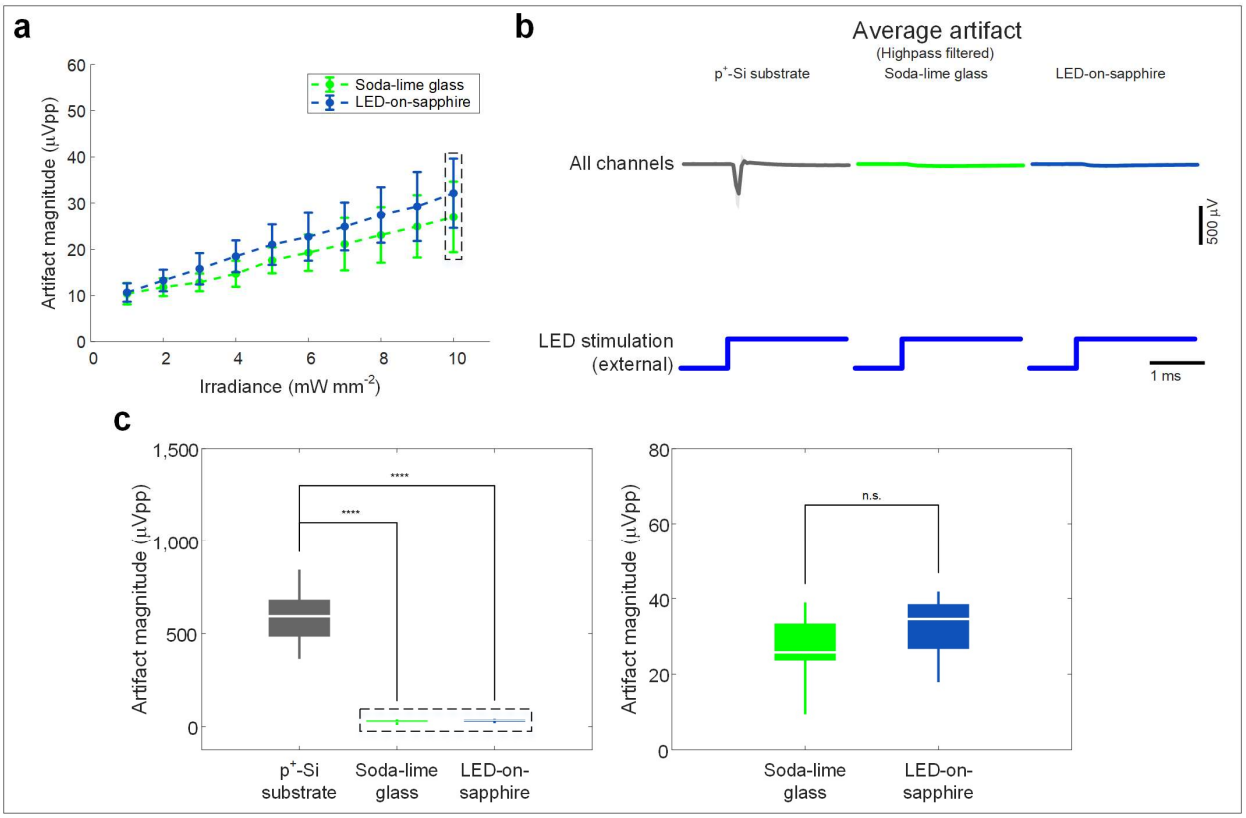

Supplementary Figure 3: PV-induced voltages measured from electrodes on the electrode arrays fabricated using non-silicon substrates. (a) Mean peak-to-peak magnitude of the high-pass filtered PV-induced voltage signal recorded from all the recording channels on electrode arrays fabricated using soda-lime glass substrate and LED-on-sapphire substrate. X coordinates indicate the irradiance of at the surface of the electrode array, and the error bars indicate one standard deviation. n = 20 and 26 for electrode arrays fabricated using soda-lime glass substrate and electrode arrays fabricated using LED-on-sapphire substrate, respectively. (b) Average high-pass filtered waveforms of PV-induced voltage signal recorded from all the recording channels on the electrode arrays, shown next to the average high-pass filtered waveform of PV-induced voltage signal recorded from the µLED optoelectrodes fabricated with p^+-Si substrate. The irradiance of the LED illumination on the optoelectrode surface was 10 mW mm^{-2}. The shaded regions show one standard deviation away from the mean and the blue traces at the bottom indicate the signal provided to the fiber-coupled LED. Lack of the high-magnitude transient artifact on

electrodes on both electrode arrays is notable, suggesting that the source of the stimulation artifact that results in the large-magnitude transient artifact on the μLED optoelectrodes is neither PV effect form the LED layer nor PEC effect on the electrode. (c) Peak-to-peak magnitudes of the signals whose averages are plotted in part b. The right panel shows the magnified view of the region inside the rectangle with black dashed sides on the left panel. Boxes indicate interquartile ranges, white lines medians, and whiskers extreme values. Mann-Whitney U test was used, n.s. indicates $p > 1.67 \times 10^{-3}$, and **** indicates $p < 3.33 \times 10^{-5}$. The mean (± SD) peak-to-peak magnitudes are 589.72 (± 125.64), 27.00 (± 7.64), and 32.14 (± 7.49) μVpp for the optoelectrodes with p^+-Si substrate (n = 56), the electrode arrays fabricated using soda-lime glass substrate (n = 20), and the electrode arrays fabricated using LED-on-sapphire substrate (n = 26), respectively. Lack of the high-magnitude of the transient artifact in the PV-induced voltage signal on the devices with non-silicon substrate is notable.

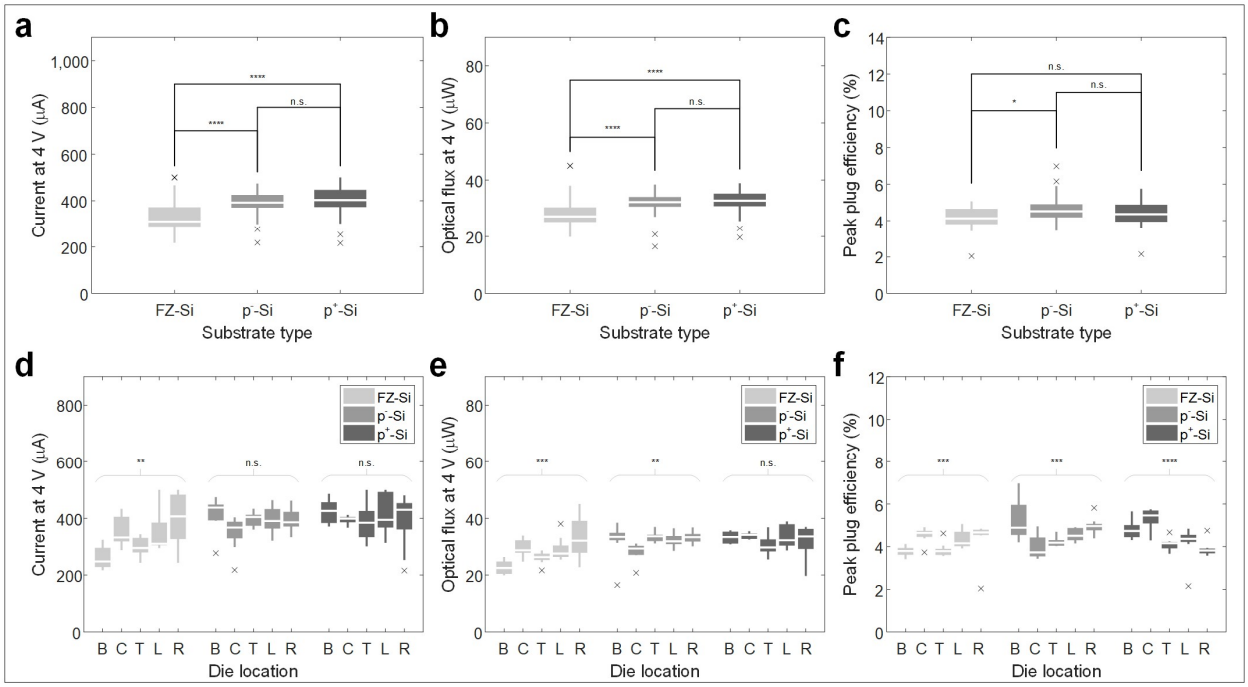

Supplementary Figure 4: Electrical and optical characteristics of μLEDs fabricated using GaN-on-Si LED wafers with silicon substrates with different boron doping densities. (a) Current flowing through μLEDs at 4 V of forward bias voltage. (b) Output optical flux of the μLEDs at 4 V of forward bias voltage. (c) Peak plug efficiency of the μLEDs. Mann-Whitney U-test was used, n.s. indicates $p > 1.67 \times 10^{-2}$, * indicates $3.33 \times 10^{-3} < p < 1.67 \times 10^{-2}$, and **** indicates $p < 3.33 \times 10^{-5}$. n = 43, 44, and 43 for μLEDs fabricated on FZ-Si substrate, p^--Si substrate, and p^+-Si substrate, respectively. (d-f) electrical and optical characteristics identical to those reported in parts a-c measured from μLEDs on different locations on the wafer. Each alphabet indicate the same location on each wafer. Kruskal-Wallis test was used, n.s. indicates $p > 0.05$, ** indicates $0.001 < p < 0.01$, *** indicates $1 \times 10^{-4} < p < 0.001$, and **** indicates $p < 1 \times 10^{-4}$. n = 8.67 ± 0.62 (mean ± SD) for each location on each wafer. While there is some difference in the electrical and optical characteristics of the μLEDs among those fabricated on wafers with different boron doping densities, significant variation of the optical and electrical characteristics among the LEDs that were fabricated on the same wafer at different location is also observed. It can be understood that

the (non-)uniformity in the LED epi-layer growth process affects the quality of the μLEDs as significantly as the dopant density in the substrate does.

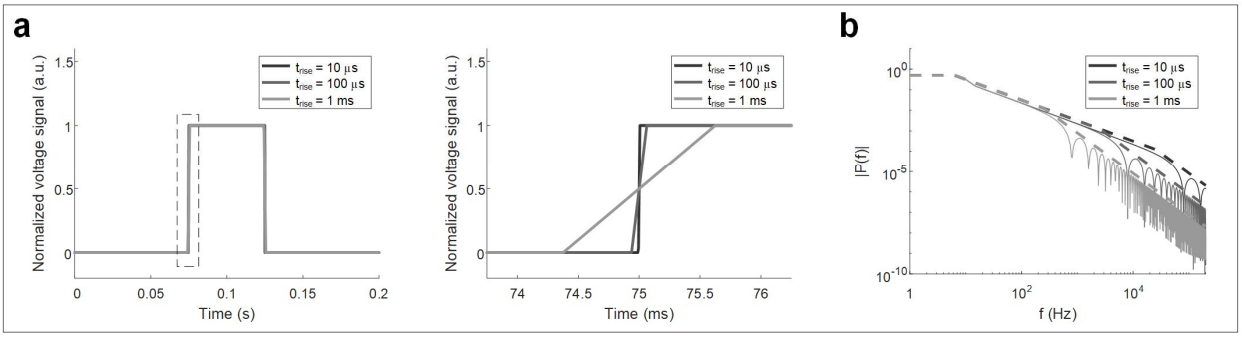

Supplementary Figure 5: Voltage pulses with different rise times and their spectra. (a) Time-domain plot of voltage pulses with (10 - 90 %) rise times of 10 μs, 100 μs, and 1 ms. The right panel shows the magnified view of the region inside the rectangle with black dashed sides on the left panel. (b) Frequency spectrum of the pulses shown in part a, showing both the envelope (in dashed lines) and the values evaluated at a few selected harmonic frequencies (in thin solid lines. Only prime numbered harmonics (f = 5 × (2, 3, 5, 7, etc.)) are shown for better visibility). Great reduction of the magnitude of the harmonics in frequencies between 250 Hz and 10 kHz is visible in the spectrum of the pulses with longer rise time, suggesting reduction of transient component of the stimulation artifact with increased slew rate and therefore smaller magnitude of the EMI-induced stimulation artifact.

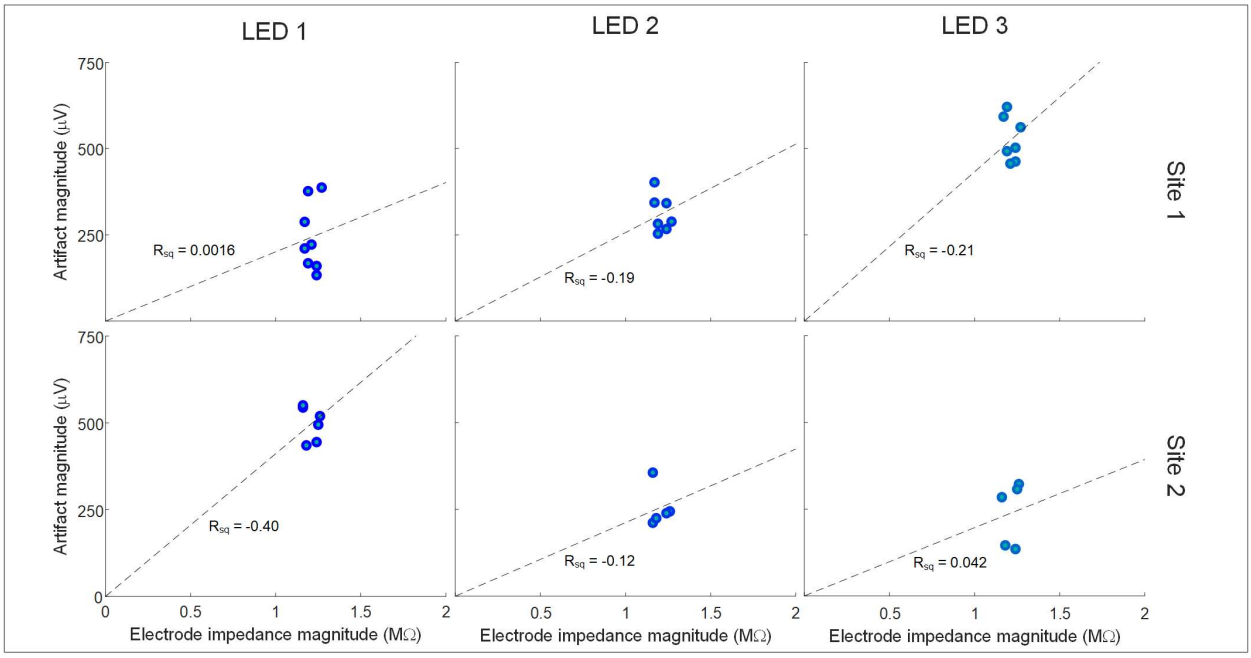

Supplementary Figure 6: Lack of correlation between recording electrode impedance and stimulation artifact magnitude. Peak-to-peak magnitude of transient stimulation artifact resulting from rectangular LED input voltage signals with 3.5 V peak-to-peak amplitude ($V_{low\text{-}level}$ = 0 V, t_{rise} = 5 ns) recorded from the sites 1 and 2 (the bottommost sites) with different impedance magnitudes are plotted. All impedances are evaluated at 1 kHz. Small R_{sq} values suggest lack of clear correlation between the artifact magnitude and the electrode impedance.

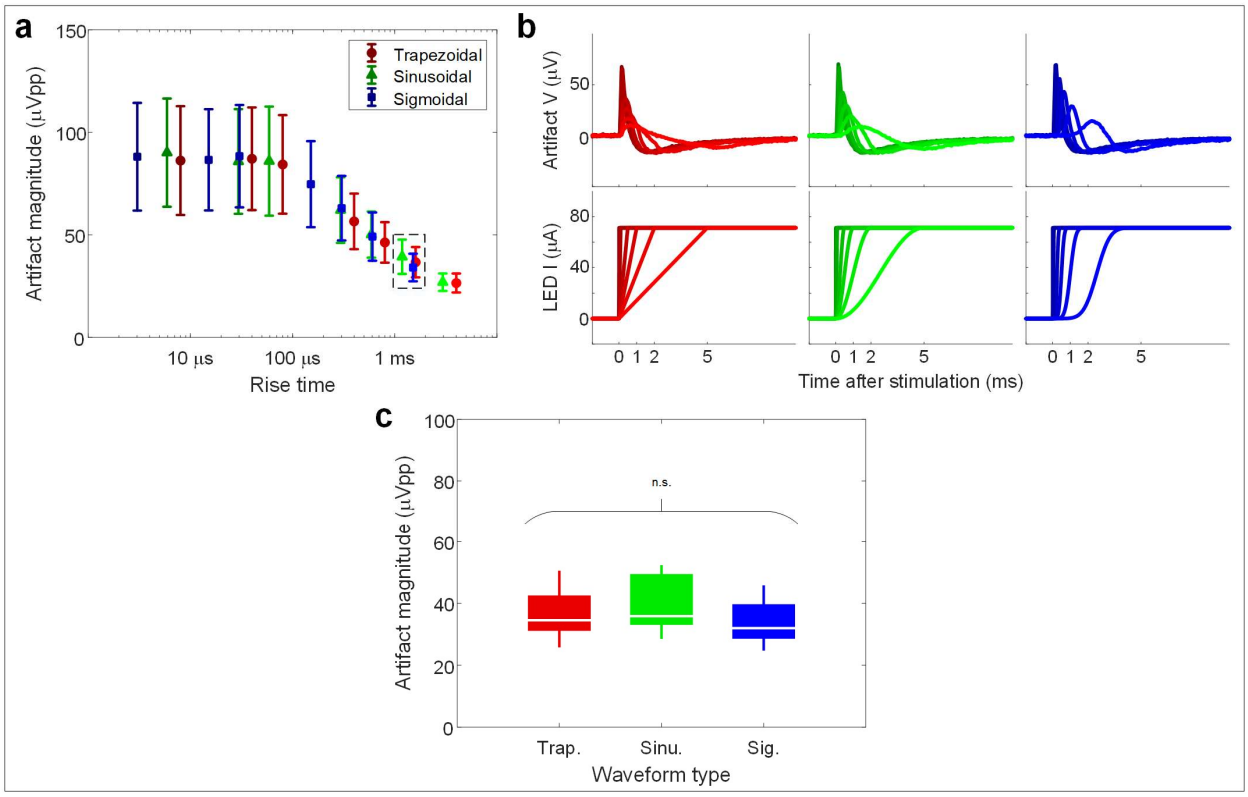

Supplementary Figure 7: Artifact resulting from stimulation with current-driven LEDs. (a) Mean peak-to-peak magnitude of the high-pass filtered stimulation artifact recorded from the channels on the µLED optoelectrodes on the shank on which a µLED was turned on. The locations of the electrodes and the interconnects from which the signals were recorded are identified in Fig. 8a. X coordinates indicate the 10 - 90 % rise time of the pulse. Circular markers indicate the average magnitudes of the stimulation artifact resulting from stimulation using trapezoidal current pulses, triangular markers those from using sinusoidal current pulses, and rectangular markers those from using sigmoidal (error function) current pulses. Error bars indicate one standard deviation (n = 18). (b) Average waveforms of the recorded stimulation artifact, whose mean peak-to-peak magnitudes are shown in part a, and the input current signal. (c) Magnitude of the high-pass filtered stimulation artifact signals whose peak-to-peak magnitudes are shown in the rectangle with black dashed sides in part a. Kruskal-Wallis test was used, and $p = 0.093$. No significant difference in the magnitude of the stimulation artifact, other than slight

shift in location of the peak of the stimulation artifact signal, is observed when current signals with different shapes were used.